Applied Thermal Engineering 184 (2021) 116264

Contents lists available at ScienceDirect

Applied Thermal Engineering

journal homepage: www.elsevier.com/locate/apthermeng

Multiphase-thermal simulation on BOG/BOR estimation due to phase change in cryogenic liquid storage tanks

Gyu-Mok Jeon [a], Jong-Chun Park [a,*], Seongim Choi [b]

[a] Dept. of Naval Architecture and Ocean Engineering, Pusan National University, Republic of Korea
[b] Dept. of Aerospace and Ocean Engineering, Virginia Tech., USA

ARTICLE INFO

Keywords:
Cryogenic liquid
Boil-off gas (BOG)
Boil-off rate (BOR)
Phase change model
Computational Fluid Dynamics (CFD)

ABSTRACT

The purpose of the study is the high-precision, numerical calculation of the Boil-off-Gas (BOG) and Boil-off-Rate (BOR) of cryogenic liquid for the design of containment cargo system (CCS) by using high-fidelity multi-physics CFD simulation of heat transfer of insulation system and phase change of multiphase-thermal flow in the cryogenic liquid tank. The results are compared with those predicted by the conventional low-fidelity methods which are based only on the total heat transfer and does not consider detailed physics related to the phase change of the cryogenic liquid in the storage tank. The unsteady Reynolds-averaged Navier-Stokes (URaNS) equations with the realizable k-ε turbulence model and the Rohsenow boiling model for phase change calculation are solved by commercial software of STAR-CCM+. First, for the validation of the phase change model, the cryogenic liquid stored in an independent tank of type C is calculated to study thermal fluid behaviors inside the tank and the corresponding values of BOG and BOR are compared with the experiments as well as the results from numerical simulations by other researchers. The estimated BOR value showed an excellent agreement with discrepancy less than 1%, resolving precisely the thermal convection caused by the vaporization of the cryogenic liquid. Subsequently, the multiphase-thermal flow in a membrane-type LNG (liquefied natural gas) storage tank was calculated for the BOR estimation, coupled with thermal conduction through the insulation system. It is concluded from those simulations that the high-fidelity CFD calculation with the phase change model was able to precisely predict the vaporization of the cryogenic liquid and to calculate the correct BOR values based on the actual BOG amount.

1. Introduction

A variety of environmental regulations are currently introduced by International Maritime Organization (IMO) in pace with the global movement of environmental protection. During the 70th Maritime Environment Protection Committee (MEPC) meeting, the International Maritime Organization (IMO) Low Sulphur Regulation was implemented and requires since Jan 2020 that all shipping companies should not emit Sulphur oxides more than 0.5% (previously 3.5%). Although the use of low Sulphur fuels or the installation of scrubbers to remove Sulphur oxide residue from the emission gas was proposed as a mitigation method, it is not the most economical solution viable in a long term. Alternatively, a clean energy fuel such as LNG or hydrogen can be effective in economy and environment.

The liquefied gas is best to be transported in liquid state through the liquefaction as it has large specific volume and remains in gaseous state at room temperature. As it is a cryogenic fluid with its boiling point lower than 120 K, it is critical to insulate the storage tank with a high-performing insulation system to minimize heat transfer from outside, while there are no materials with 100% insulation capacity, and the BOG due to the phase change of the cryogenic liquid and natural vaporization are inevitable. In Fig. 1, external heat is transferred into the insulation panel and the heat convection begins from the fluid on the contact surface of the insulation panel. Vaporization occurs on the contact surfaces of vapor–liquid and solid–liquid interfaces, and the BOG is defined as the total amount of the vaporized gas [13]. Factors contributing to the BOG besides the external heat transfers include changes in local pressure due to sloshing, cargo changes from loading and unloading, heat transfer from the entrance/exit areas, and environmental changes in pressure and temperature outside the storage tank. The biggest contribution is the change in thermal energy by the external heat transfer, and the amount of BOG over a single day is

* Corresponding author.
E-mail address: jcpark@pnu.edu (J.-C. Park).

https://doi.org/10.1016/j.applthermaleng.2020.116264
Received 25 July 2020; Received in revised form 12 October 2020; Accepted 24 October 2020
Available online 5 November 2020

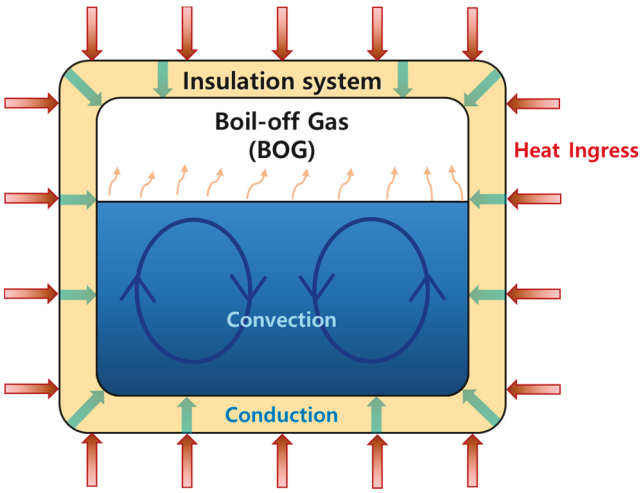

Fig. 1. Schematic representation of boil-off gas and thermal flow in cryogenic tank with insulation system from heat ingress.

defined as the BOR [46]. The BOR is one of the key parameters to represent the design performance of the CCS.

The emission of the BOG from the cryogenic storage tank due to external heat from the environment leads to potential loss in economy, and the re-liquefaction or the natural process has been proposed as a mitigation approach. However, the capacity of re-liquefaction facility and the details of the natural process are determined by the total amount of the BOG generated by the vaporization [17,26]. The design of CCS for the cryogenic liquid is greatly affected by the BOR which is proportional to the BOG. Therefore, for the design of efficient CCS and to determine the capacity of the re-liquefaction facility and the details of the process, it is most important to predict the exact values of BOG and BOR in the cryogenic liquid storage tank.

Experimental studies have been previously carried out for the accurate prediction of the BOG and BOR [7,24,25,23,6,33,8,29]. In experiments, most of the liquefied gas are inert gas such as nitrogen and helium due to avoiding the danger of explosion. However, the liquefied gas used as the fuel in industry and life are active gas like LNG and hydrogen and they are hard to handle and control in experiment. Additionally, experimental investigations are based on lab-scale prototypes, and they cannot mimic the actual state of large static pressure of a full-scale tank, which means boiling temperature is difference due to the discrepancy in the static pressure. In addition, it has a problem to change the ratio of surface area to volume, for example when the experimental tank is scaled down by 100:1, the surface area to volume ratio will be larger by 100 times. The difference of surface area to volume ratio have an influence on the heat transfer characteristics and internal flow dynamics in the tank. It seems to be impractical for investigating experimentally BOG and BOR in the full-scale tank. In addition, most of the types of liquefied gas used in experiments are nitrogen or helium, which is a strong constraint to represent liquid in reality. Therefore, the CFD simulation is more realistic alternative for estimating BOR and BOG enabling graphical visualization of physics as well as quantitative assessment of flow variables to provide invaluable insights in physics [39].

A conventional numerical analysis method to estimate the BOR neglects the fluid inside the storage tank and employs a simple thermal equilibrium state on the insulation system to calculate the total heat leakage [31,14,34,20,33]. There are recent studies on thermal analysis based on the total heat transfer made to the insulation system considers the phase change of the liquefied gas [19] and the corresponding heat convection phenomena, which makes the method difficult for simulation involving the sloshing during ship operation [36]. However, this method cannot be applied the condition, which involves the difficult problems for true physics simulation especially cargo-filling changes during loading/unloading.

The CFD methods have been used to solve multi-phase problems that are often encountered in diverse areas of chemical process, nuclear power, automotive industry, and aerospace engineering. Krepper et al. [27,28] developed a two-phase CFD model to simulate the formation of micro-scale bubbles in a nuclear reactor, and numerical results were in reasonable agreements with experiments. Banerjee [4,5] developed a phase change model using the Volume-of-Fluid (VOF) model and solved stratified flows in a two-dimensional channel having an oblique edge and calculated the effects on the phase change by the temperature, velocity, and humidity relative to vapor as well as the temperature of inlet in liquid state. Hassanvan et al. [16] carried out the CFD simulation of the gasoline vaporization in the fuel tank of the car during the splash loading, and compared numerical results to theoretical values with good agreements. The simulation of the vaporization of the cryogenic liquid using the phase change model has been studied by Lee et al. [32], Fu et al. [12]. Lee et al. [32] simulated the leakage of the LNG from the membrane type tank, and employed a diffusion-based model to identify the phase change of the liquefied gas through the porous structure. After Lee et al. [32] developed the phase change model in ANSYS Fluent, many relative researches were recently conducted and improved the code [47,11,48,44,43,49]. Fu et al. [12] carried out CFD simulation of the phase change of the liquid hydrogen in the fuel tank of the spacecraft caused by the gravity and the surface tension, and verified that the gas bubbles generated by the vaporization affects the internal pressure of the tank. Zakaria et al. [46] calculated the BOG of the full-scale cargo ship tank, but the description of the geometry and details on the numerical analysis was not included. Ahammad et al. [2] carried out a numerical study on the vaporization frequency of the liquid nitrogen and LNG at the time of the film boiling inside the cryogenic storage tank, and visualized the physics for the detailed analysis that cannot be identified by experiments. Langari et al. [30] carried out the CFD simulation of the subcooled boiling flows in the horizontal duct. They concluded that numerical results from the large eddy simulation (LES) and from the Reynolds-averaged Navier-Stokes (RaNS) with turbulence models are similar and do not show much differences from the experiments. Saleem et al. [39] used the CFD methods for the simulation of the BOG in the full-scale onshore LNG storage tank and analyzed the effects of the numerical parameters of the phase change model on the results. A recent study by Chen [9] used the phase change model in the multiphase fluid models of Eulerian Multiphase (EMP) and Volume-of-Fluid (VOF). Temperature and heat flux distribution were compared for the two models with no major differences. Majority of the aforementioned studies conducted the numerical effects of input parameters of the phase change model and modifications in the boundary conditions, however; a quantitative comparison with the experiments is few.

A reliable study has been reported to date which calculate the BOG and BOR using the phase change model in the cryogenic storage tank with the insulation system, and includes the validation study with the existing experiment [29]. Krikkis [29] compared their simulation results by the thermodynamic and heat transfer model with measurement data of temperature in the insulation, and pressure and boil-off rate in membrane tank.

In the present study, a high-precision CFD simulation is carried out to calculate multi-phase thermal flow solutions as well as heat transfer on the insulation system in the CCS of the cryogenic liquid. The BOR is estimated based on the BOG values calculated by the multi-phase CFD analysis, and compared with results from the traditional methods which are based on the amount of total heat transfer only. First, for the validation of the phase change model in the CFD analysis, the liquid nitrogen in the independent tank of type C is solved for the BOG and BOR with detailed analysis on the characteristics of internal thermal fluids, and the results are compared with experimental and other numerical results [33]. Subsequently, LNG in the membrane-type KC-1 tank is

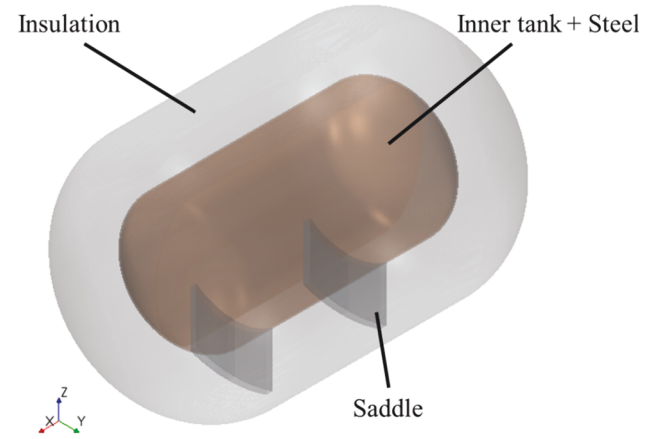

(a) Sketch of C-type tank

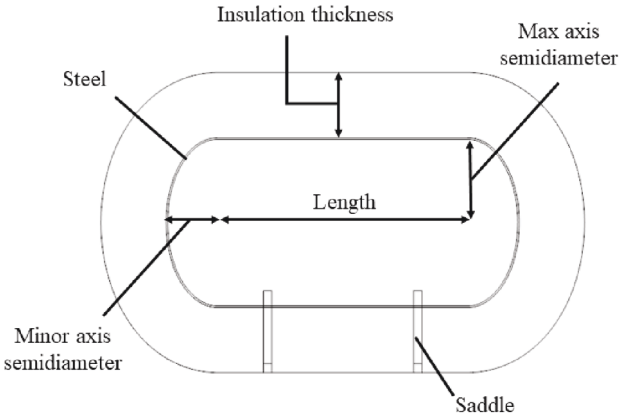

(b) Layout of LN_2 tank

Fig. 2. Geometry of C-type independent tank.

Table 1
Dimension of LN_2 tank.

Item	Unit (mm)
Thickness of insulation	400
Thickness of steel	10
Thickness of saddle	50
Minor axis semidiameter	300
Maximum axis semidiameter	500
Length	1500

Table 2
Thermal properties of LN_2.

	Enthalpy of vaporization (kJ/kg)	Density (kg/m^3)
LN_2	198.6	808.3

Table 3
Thermal properties of nitrogen.

	Conductivity (W/(m·K))	Specific heat (J/kg·K)	Density (kg/m^3)
Nitrogen	0.009	1038	1.25

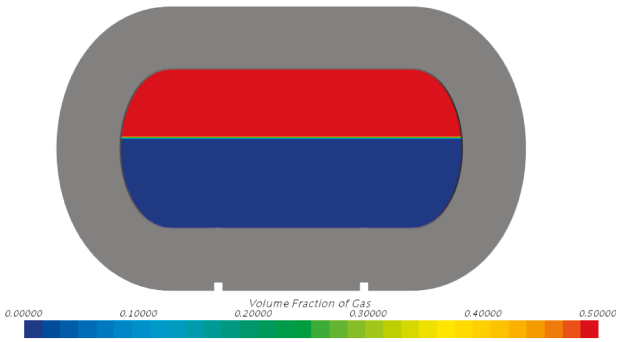

(a) Volume of fraction

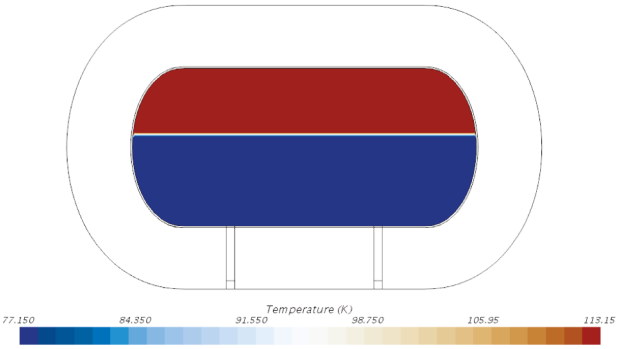

(b) Temperature distribution (Fluid)

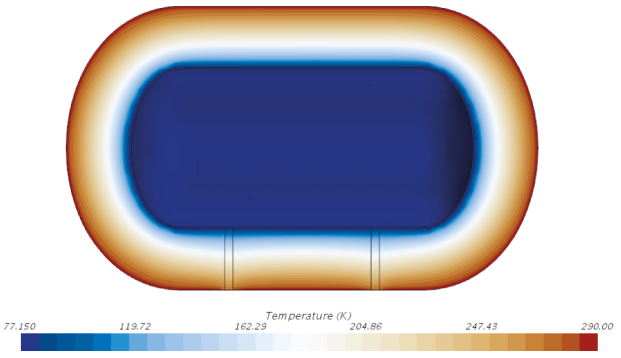

(c) Temperature distribution (Solid)

Fig. 3. Initial conditions.

Table 4
Initial temperature of fluid.

	Liquid nitrogen	Nitrogen
Temperature (K)	77.15	113.15

Table 5
Thermal properties of tank.

	Conductivity (W/(m·K))	Specific heat (J/kg·K)	Density (kg/m^3)
Insulation	0.023	28	45
Steel	8.72	499	7850
Saddle	0.4	1720	1100

solved for the BOG using the CFD analysis with the phase change model. The results are compared with those of other numerical simulations [34,45,20].

2. Mathematical model

2.1. Governing equation

A multi-physics CFD simulation is carried out which takes into ac-

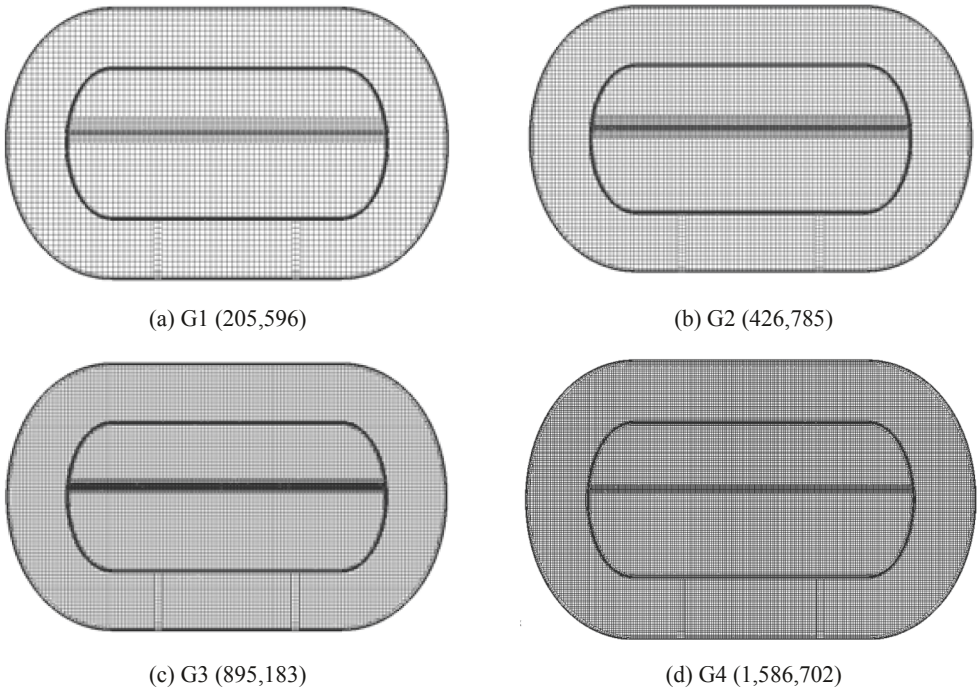

(a) G1 (205,596) (b) G2 (426,785)

(c) G3 (895,183) (d) G4 (1,586,702)

Fig. 4. Grid system.

count both the heat conduction on the insulation and the multi-phase characteristics of the cryogenic liquid in the storage tank. The cryogenic multi-phase thermal flows are assumed governed by three-dimensional unsteady viscous flows with compressible effects, and only the phase change is calculated with internal chemical reaction neglected. The phase change model in the VOF method is employed to analyze vaporization on the contact surfaces of liquid and gas. The VOF method uses the same equations in conservation form for gas in both liquid and gaseous states, and more efficient in computation than EMP (Eulerian Multi-Phase) model [9]. The present study uses equations of mass, momentum, and energy in conservation form which are shown in Eqs. (1), (5), and (6), respectively.

$$\frac{\partial}{\partial t}\int_V \rho dV + \oint_A \rho \mathbf{v}\cdot d\mathbf{a} = \int_V S dV \tag{1}$$

$$\sum_{i=1}^{n} \alpha_i \rho_i = \rho \tag{2}$$

$$\sum_{i=1}^{n} \alpha_i = 1 \tag{3}$$

$$S = \sum_i S_{a_i}\cdot\rho_i \tag{4}$$

where α_i is the volume fraction of phase i, ρ_i the density of phase i, $\mathbf{a}$ the surface area vector, $\mathbf{v}$ the mixture (mass-averaged) velocity and S the mass source term.

$$\frac{\partial}{\partial t}\left(\int_V \rho \mathbf{v} dV\right) + \oint_A \rho \mathbf{v}\otimes\mathbf{v}\cdot d\mathbf{a} = -\oint_A p\mathbf{I}\cdot d\mathbf{a} + \oint_A \mathbf{T}\cdot d\mathbf{a} + \int_V \rho \mathbf{g} dV + \int_V \mathbf{f}_b dV \tag{5}$$

where p is the pressure, $\mathbf{I}$ the unity tensor, $\boldsymbol{g}$ the gravity, $\boldsymbol{T}$ the stress tensor and $\mathbf{f}_b$ the vector of body forces

$$\frac{\partial}{\partial t}\int_V \rho E dV + \oint_A (\rho \mathbf{H}\mathbf{v} + p)\cdot d\mathbf{a} = -\oint_A \dot{\mathbf{q}}'' d\mathbf{a} + \oint_A \boldsymbol{T}\cdot\mathbf{v} d\mathbf{a} + \int_V \boldsymbol{f}_b\cdot\mathbf{v} dV + \int_V S_E dV \tag{6}$$

where E is the total energy(=internal energy + kinetic energy), H the total enthalpy, $\dot{q}''$ the heat flux vector and S_E the energy source term. In each term of mass source term (S) in continuity equation and energy source term (S_E) in energy equation, the phase change term is used to estimate the mass transfer from one phase to another and to compute the heat transfer during evaporation.

The equation of energy for solid to analyze the heat transfer on the insulation of the cryogenic storage tank.

$$\frac{\partial}{\partial t}\int_V \rho_s C_p T_s dV = -\oint_A \dot{\mathbf{q}}'' d\mathbf{a} + \int_V S_u dV \tag{7}$$

where ρ_s is the solid density, C_p the specific heat, T_s the solid temperature and S_u the volumetric heat source within the solid. Based on the conservation of energy, total heat flux is conserved across the fluid–solid interface. At a contact interface, conjugated heat transfer interface is applied.

The governing equations of (1), (5), (6), and (7) are discretized by the finite volume method (FVM). For the CFD analysis, commercial CFD software of STAR-CCM+ [41] is used to solve the heat transfer of the insulation and the multi-phase thermal fluids. A 2nd order accurate implicit method is used for the temporal integration with a variable time step method controlling the Courant-Friedrichs-Lewy (CFL) number. The average CFL number is set 0.2 to minimize numerical instability that may occur on the free surface. Also, a 2nd order central differencing with second order upwind in spatial discretization is applied in the simulation.

2.2. Phase change model

The phase change model implemented in the STAR-CCM+ software is composed of the EMP boiling model and the VOF boiling model in Eulerian model. The EMP boiling model is known to be the best in solving the fine bubbles from the vaporization of the cryogenic liquid in the storage tank. However, the solution of fine bubbles in the full-scale tank requires a computational mesh of enormously high resolution and exorbitant computing power. In the present study, the VOF boiling model [38] is employed for the simulation of phase change of the

liquefied gas as it can solve bubbles with much larger mesh size and becomes more efficient.

The phase change model of the VOF boiling method applies different solution approach to the liquid–solid and the liquid–vapor interfaces. For the liquid–solid interface, the wall temperature should be higher than the saturation temperature to activate the phase change model, and the vapor mass generation rate ($\dot{m}_{ew}$) in the liquid–solid interface is represented as follows.

$$\dot{m}_{ew} = \frac{C_{ew} q_{bw}}{h_{lat}}, \tag{8}$$

where C_{ew} is the model constant starting how much of the boiling heat flux is used for creation of vapor bubbles, h_{lat} the latent heat and q_{bw} the heat flux at wall due to phase change, which is given by:

$$q_{bw} = \mu_l h_{lat} \sqrt{\frac{g(\rho_l - \rho_v)}{\sigma}} \left(\frac{C_{p_l}(T_w - T_{sat})}{C_{qw} h_{lat} Pr_l^{n_p}} \right)^{3.03} \tag{9}$$

where μ_l is the dynamic viscosity of liquid, C_{p_l} the specific heat, Pr_l the Prandtl number of the liquid phase, n_p the Prandtl number exponent, σ the surface tension coefficient, T_w the wall temperature, T_{sat} the saturation temperature and C_{qw} the empirical coefficient varying with the liquid-surface combination

Next, when the temperature of the vapor on the liquid–vapor interface reaches T_{sat}, with some discrepancies from the temperature of the liquid–vapor mixture (T), all the heat flux from the liquid to the interface is used in mass transfer. The mass transfer caused by heat transfer to the interface between the media is used to compute the rate of phase change as below.

$$\dot{m}_{ec} = \frac{C_{heat}(T - T_{sat})}{h_{lat}} \tag{10}$$

where C_{heat} is the heat transfer coefficient between the vapor bubbles and surrounding liquid and is related to the resolution of the fluid flow – whether the bubbles are accurately captured or if it is assumed that small bubbles are distributed throughout the fluid. A common expression for C_{heat} is:

$$C_{heat} = \frac{k_l}{d_v} Nu_v \cdot A_i \tag{11}$$

$$A_i = \frac{6}{d_v} \alpha_l \alpha_v \tag{12}$$

where k_l is the thermal conductivity of the liquid, d_v the vapor diameter, Nu_b the Nusselt number of the vapor, A_i the interface area concentration, α_l the volume fraction of liquid and α_v the volume fraction of vapor. To assume the spherical shape vapor, the Ranz-Marshall correlation [37] is applied to calculate the Nusselt number. In the present simulation, the Ranz-Marshall correlation was used for the gas and liquid [18]. The correlation is given as:

$$Nu_v = 2 + 0.6 Re_{slip}^{0.5} Pr^{0.3} \tag{13}$$

$$Re_{slip} = \frac{V_{slip} d_v}{\nu_l} \tag{14}$$

$$Pr = \frac{\mu_l \cdot c_p}{k_l} \tag{15}$$

where Re_{slip} is the slip velocity Reynolds number, V_{slip} the slip velocity between liquid and vapor, ν_l the kinematic viscosity of liquid and c_p the specific heat.

2.3. Turbulence model

A non-dimensional, Reyleigh number, Ra, is defined as follows to determine the intensity of turbulence of thermal fluids due to the heat transfer from external sources.

$$Ra = \frac{g\beta}{\nu k}(T_2 - T_1)x^3 \tag{16}$$

where β is the thermal expansion coefficient, x the characteristic length, ν the kinetic viscosity, k the thermal diffusivity, T_1 the fluid temperature far from the surface of the object, T_2 the surface temperature.

As the size of the full-scale cryogenic storage tank is large in diameter and height, the Rayleigh number is also high and the flows are assumed

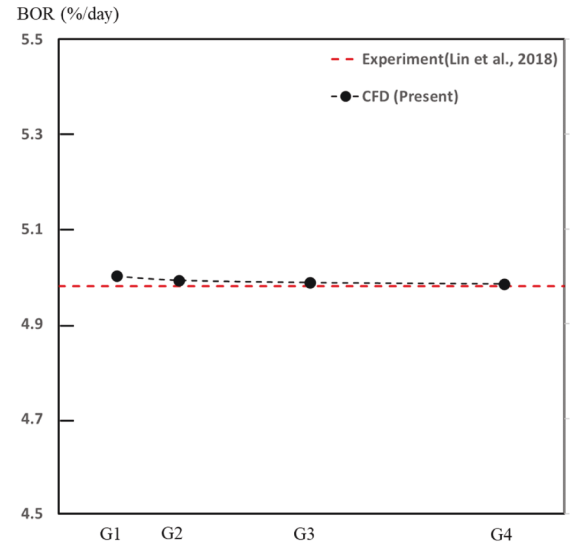

(a) Boil-off rate

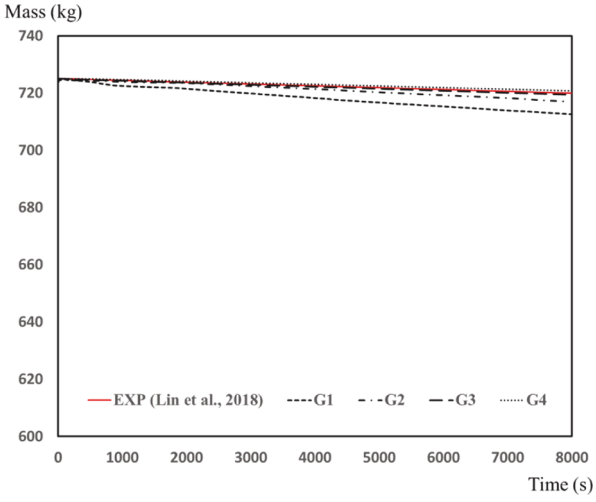

(b) Boil-off gas

Fig. 5. Grid convergence test.

Table 6
Boil off rate and difference with experimental results in grid convergence test.

Case	Number of grids	BOR_Q (%/day)	Difference (%)
G1	205,596	5.001	0.59
G2	426,785	4.992	0.24
G3	895,183	4.987	0.14
G4	1,586,702	4.984	0.08

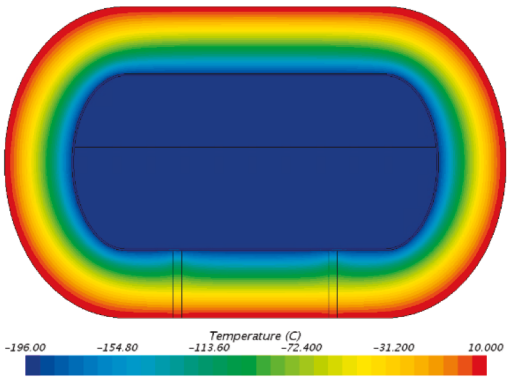

(a) overall distribution

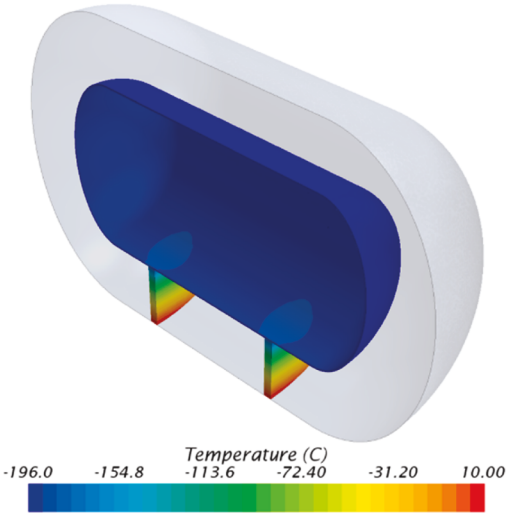

(b) near saddle at t=5500sec

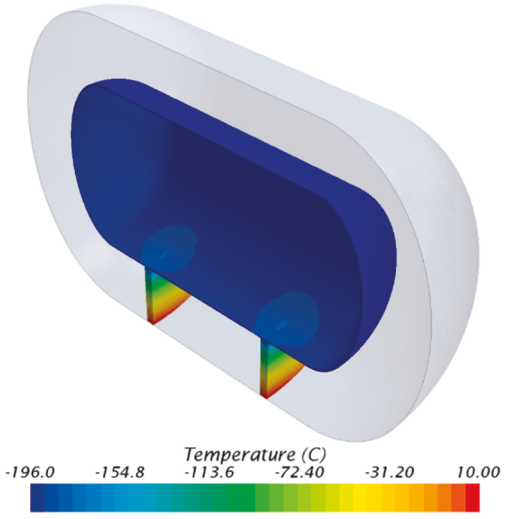

(c) near saddle at t=8000sec

Fig 6. Temperature distribution.

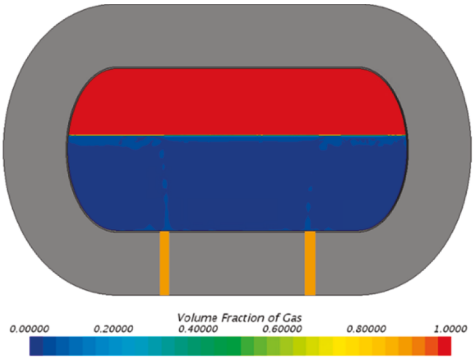

(a) 5500s

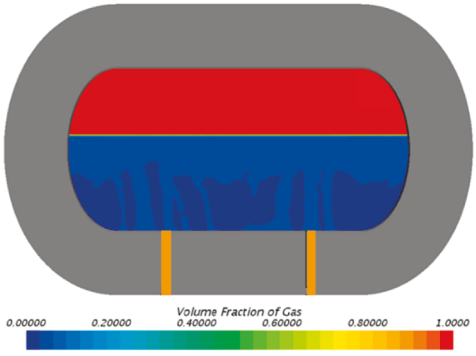

(b) 8000s

Fig. 7. Volume fraction of gas in tank.

to be turbulent [23]. However, the present study includes a cryogenics storage tank in experiment scale, it is necessary to check for turbulence by the Rayleigh number. Characteristics lengths of the type C and membrane tanks, which will be discussed in the following section, are the maximum axis diameter and the distance from the top to bottom of the tank, respectively. Corresponding Rayleigh numbers are 6.03E+13 and 2.41E+15 for the type C and the membrane tank.

For the turbulence model of the URaNS solver, one of the two-equation models, realizable k-ε model [40] is used based on the study by Langari et al. [30]. For the analysis of thermal fluids due to the natural convection on the walls, the model of the Buoyancy-Driven Two-Layer type [42] is used to solve thermal boundary layer flows.

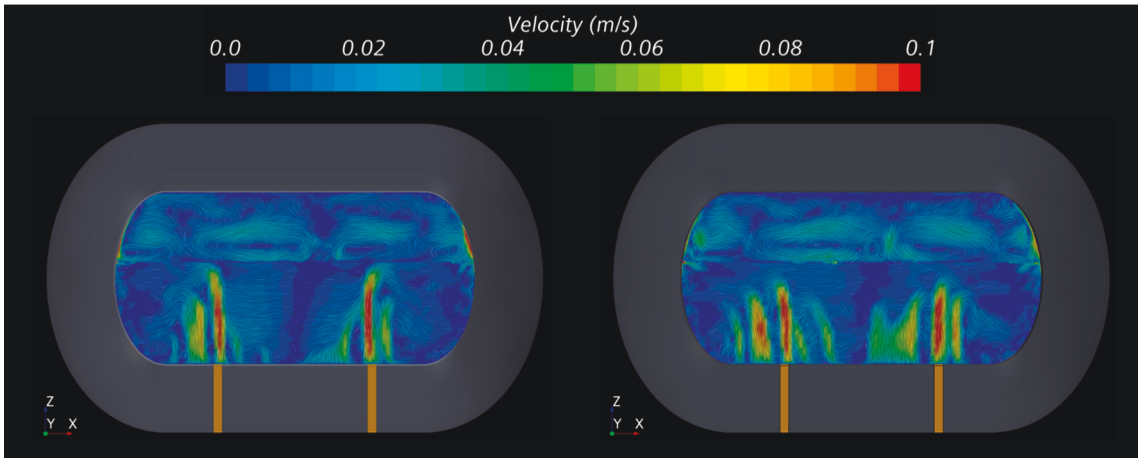

(a) 5500s (b) 8000s

Fig. 8. Velocity vector field in tank.

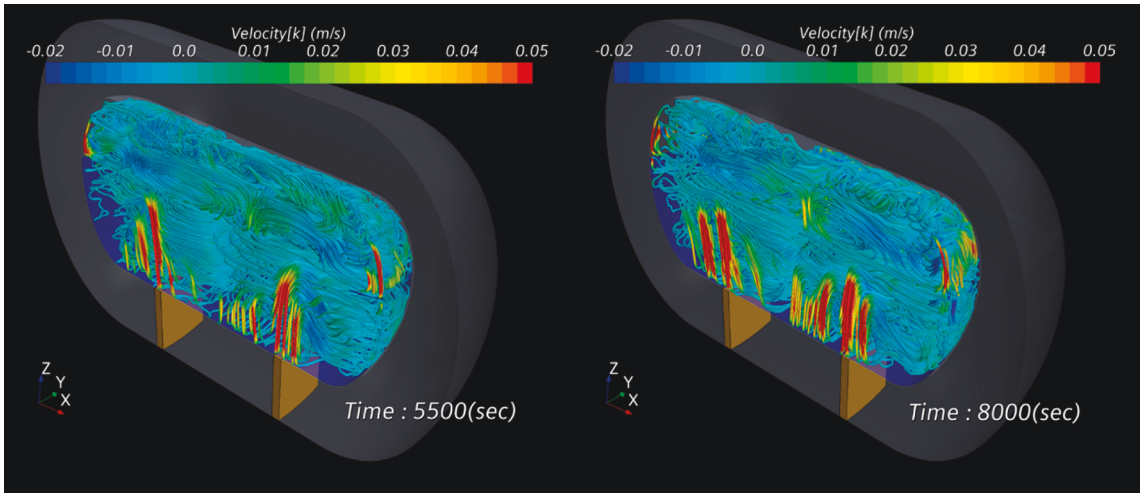

(a) 5500s (b) 8000s

Fig. 9. Streamline with velocity [k] in tank (ISO view on the symmetric plane).

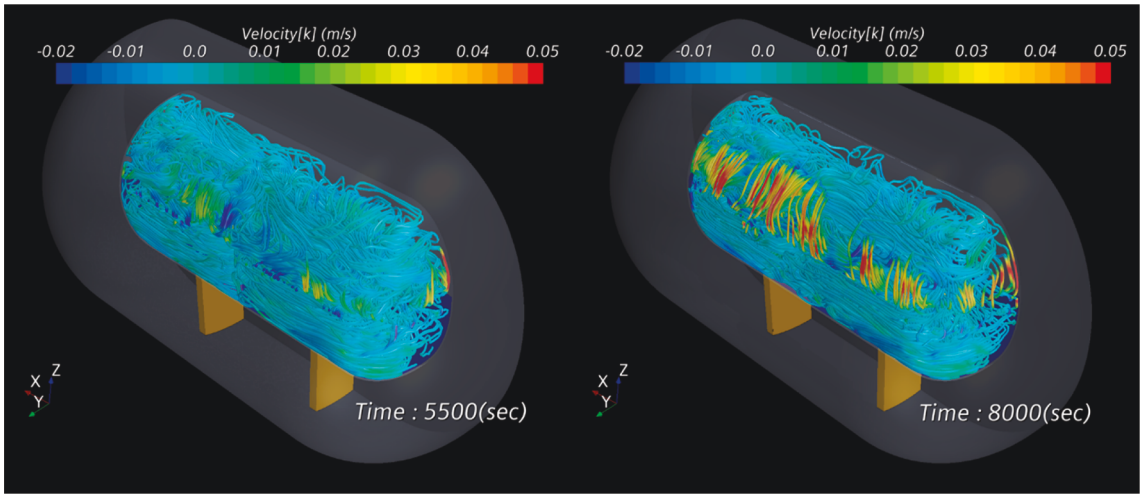

(a) 5500s (b) 8000s

Fig. 10. Streamline with velocity [k] in tank (ISO view from outside).

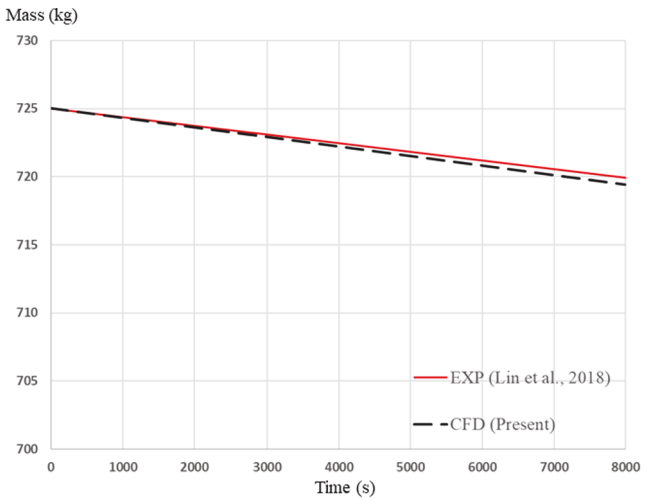

Fig. 11. Comparison of BOG with experimental data.

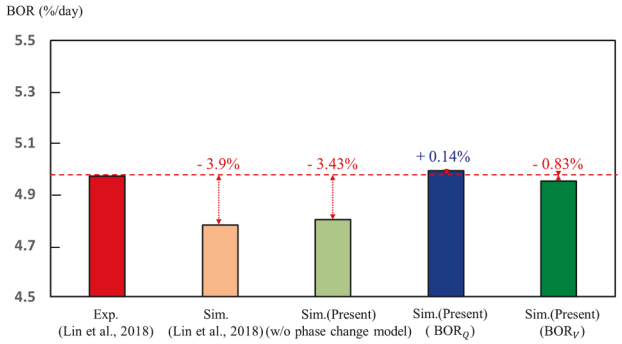

Fig. 12. Comparison of BOR with experiment and other data.

Table 7
Difference of Q_{leak} compared to experimental data.

	Experiment	Simulation [33]	Simulation w/o phase change model (Present)	Simulation w/ phase change model (Present)
Difference of Q_{leak} (W)	–	5.3	4.75	0.47

2.4. Estimation of BOR

2.4.1. Estimation of BOR_Q based on total heat transfer

Due to very low temperature of the cargo, many design factors must be taken into account when designing a gas vessel. Under ambient conditions, the heat flux into the cargo tank produces BOG. This makes pressure inside the tank increase and generate the BOG to maintain the design pressure. Therefore, it is necessary to evaluate the BOR for the cargo tank insulation system. BOR can be estimated by assuming that all heat fluxes from the outside of the cargo tank to the inside produce BOG. The daily BOR can be estimated by following equation:

$$BOR_Q = \frac{Q_{leak} \times 3600 \times 24}{\rho_l \times V_{\text{tank}} \times h} \times 100 \tag{17}$$

where Q_{leak} represents the total heat flux that penetrates into the cryogenic tank, ρ_l the liquid density, V_{tank} is the volume of tank and h the latent for vaporization. The equation to calculate Q_{leak} is as follows.

$$Q_{leak} = C_{heat\_transfer} A_{\text{tank}} \Delta T \tag{18}$$

where $C_{heat\_transfer}$ is overall heat transfer coefficient, A_{tank} the surface area of tank and ΔT difference in temperature between the surroundings and the fluid.

2.4.2. Estimation of BORv based on amount of vaporization

The estimation of the BOR based on the total heat transfer does not consider natural convection nor the phase change of the internal fluid, and thus has limitations in explaining the true physics of cryogenic liquid in the storage tank. In the present study, the estimation of the BOR is made based on the calculation of the actual BOG generated due to the phase change of the liquefied gas. The formulation for the BOR estimation is the same as that used in the study by Lin et al., [33].

$$BOR_V = \frac{\rho_g \times V_{BOG} \times 24}{\rho_l \times V_l} \times 100 \tag{19}$$

where ρ_g is the density of gas and V_{BOG} represents the volume of gas per hour. The equation to calculate V_{BOG} is as follows.

$$V_{BOG} = V_{\text{tank}}(\alpha_{gas,t_0} - \alpha_{gas,t_1}) \tag{20}$$

where V_{tank} is the volume of tank, α_{gas,t_0} the volume fraction of gas at t_0, t_0 the beginning time in constant rate of BOG and t_1 the t_0 + 3600sec.

3. Numerical simulation for BOR estimation

3.1. Validation case: C-type LN_2 tank

3.1.1. Geometry modeling

A test problem for the validation of the phase change model used in the CFD analysis is the type C tank as shown in Fig. 2. It consists of the components of the insulation, inner tank, steel and saddle, and was previously used in the study by Lin et al. [33]. In Fig. 2(b), there is an internal structure of steel between the insulation and the inner tank, and the saddle penetrates the insulation through the inner tank. Solid domains are the insulation, inner tank, steel and saddle, whereas the interior of the inner tank is defined as a fluid domain. Information on the geometric details is listed in Table 1.

3.1.2. Simulation conditions

Experimental data for the validation of the phase change model in the CFD analysis were available from the study by Lin et al. [33], and the BOR values of the type-C tank with 60% filling ratio are compared. The same thermal properties and test conditions are applied to the CFD simulation and shown in Tables 2 and 3. Initial temperatures of the liquid nitrogen and the nitrogen gas are 77.15 K and 113.15 K, respectively, which are the values measured from the experiments. When applying the initial temperature condition for the CFD calculation, a temperature distribution up to 5 cm above the free surface was set to be the same as the initial temperature of the liquid to reduce the effect of heating source. Material properties of the insulation, steel and saddle are shown in Table 5 and are needed for the analysis of the heat conduction in the type-C tank, while the temperature outside the tank is set 293.15 K. Fig. 3 shows the volume fraction of gas and liquid, temperature distribution of the fluids, and the solid, respectively, when the initial condition of the simulation is applied (see Table 4).

3.1.3. Grid convergence tests

For the CFD mesh generation, the automatic grid generation module of the STAR-CCM+ is used with trimmed cells and prism layer, and the total number of cells varies from 200,000 to 1,580,000 as shown in Fig. 4. For all meshes, grid refinement is carried out near the contact surface of the liquid and vapor in the regions about 1 cm above and 7 cm below the interface, and the domain is treated as a fluid state. Also, the simulations have been run using a 16-core Intel i9-9960X 3.10 GHz CPU. The simulation time varied between 6 days to 51 days depending on grid

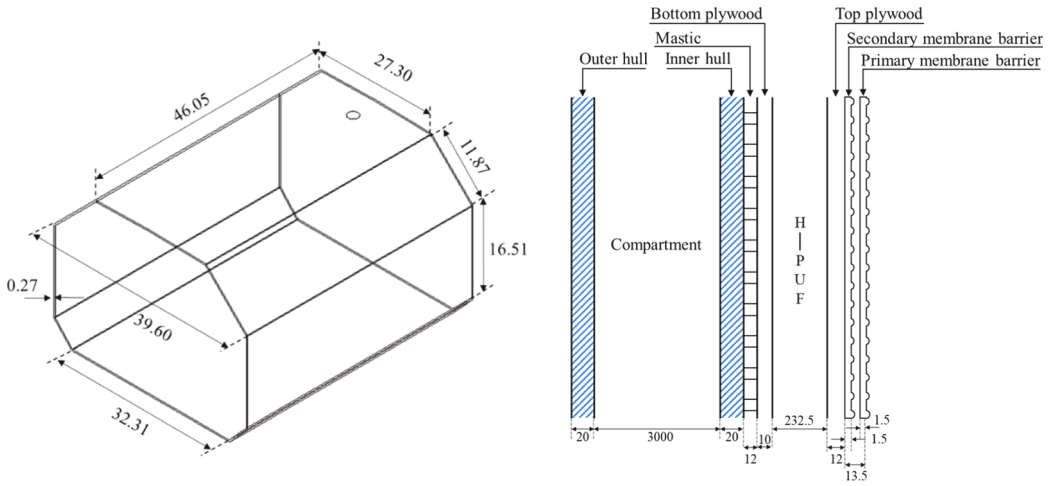

(a) Dimensions of LNG tank (b) Cross-sectional dimensions of insulation

Fig. 13. Dimensions of KC-1 membrane tank and insulation system [20].

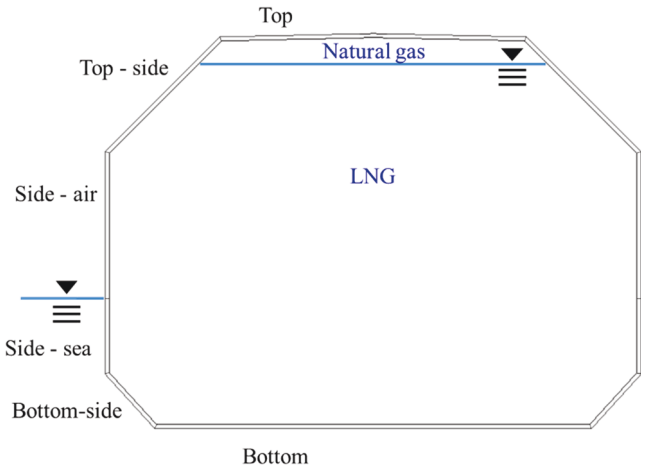

Fig. 14. Definition of boundary for setting initial temperature.

Table 8
Physical properties of insulation materials [14,22,20].

	Thickness (m)	Density (kg/m^3)	Specific heat (J/kg·°C)	Thermal conductivity (W/m·°C)
Mastic	0.01	495	1046.70	0.400
Bottom plywood	0.01	710	1088.57	0.170
H-PUF	0.2325	120	920.68	0.029
Top plywood	0.012	710	1088.57	0.170
Membrane barrier	0.0135	8137	460.54	39.000

system.

A grid convergence study is carried out for the value of BOR_Q which is estimated based on the total heat transfer and BOG compared to experimental data, and the results are shown in Fig. 5(a) and (b). Table 6 summarizes the values of BOR_Q with respect to a varying number of the grid cells along with the percentile differences in BOR_Q from the experiments. For all cases, a relative error is less than 1%, which is similar to what has been concluded in the study by Chen [9]. Also, the actual amount of BOG generated in the tank over time is converged and the results are described in Fig. 5(b). In the present study, a mesh of G3 is chosen as the it shows converged value of the BOG on the contact surfaces of vapor–liquid and solid–liquid regardless of the higher mesh resolution.

Table 10
Thermal properties of LNG.

	Enthalpy of vaporization (kJ/kg)	Density (kg/m^3)
LNG	510	425

Table 11
Thermal properties of natural gas.

	Conductivity (W/(m·K))	Specific heat (J/kg·K)	Density (kg/m^3)
Natural gas	0.0117	2199.375	1.577

Table 12
Initial temperature of fluid.

	LNG	Natural gas
Temperature (K)	110	120

3.1.4. Simulation results

The multiple physics problem of the vaporization on the contact surfaces of solid–liquid and vapor–liquid is solved by the phase change model formulated in Eqs. (8) and (10) which include the differences in saturation temperatures on the interfaces. Numerical solutions are shown in Fig. 6 of the temperature distributions inside the tank including the insulation. Fig. 6(a) shows the distribution of the temperature on the insulation of the tank as well as on the cryogenic liquid. It is shown that the temperature near the contact surface of the saddle

Table 9
Initial temperature distribution on insulation system from Jeong et al. [20].

Location	Top	Top-side	Side		Bottom-side	Bottom	Cofferdam
			Air	Sea			
Temperature (°C)	39.25	39.03	36.53	29.13	28.54	27.64	3.06

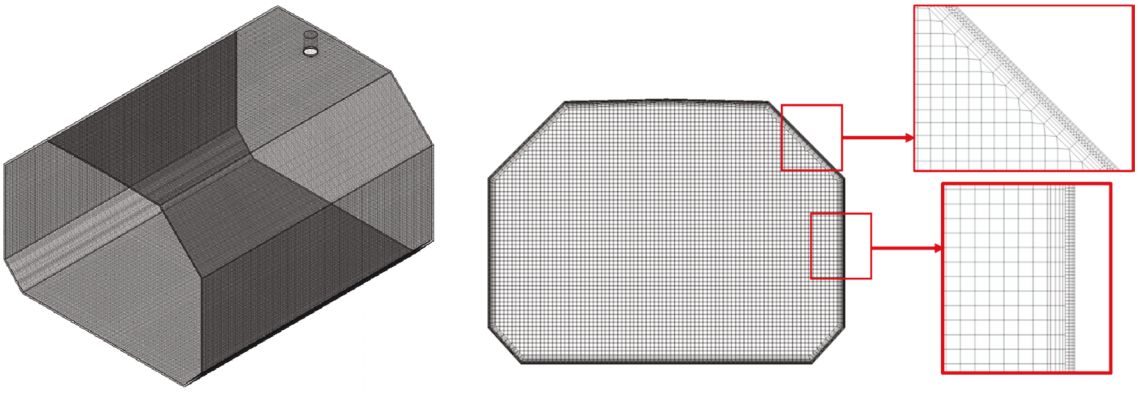

Fig. 15. Grid system for KC-1 LNG tank.

and the inner tank becomes slightly higher than that near the insulation, which is because the thermal conductivity of the saddle is higher than that of the insulation. If the external heat continues being transferred in over time, the vaporization becomes more active and the amount of vapor increases correspondingly. Changes in the temperature distributions due to the external heat transfer are shown in Fig. 6(b) and (c) at the two different times of 5500 and 8000 s, respectively. It is shown that that the surface temperature on the saddle becomes about 5degree higher than the saturation temperature of (−196 °C), which indicates that nucleate boiling is triggered in the boiling regimes [35]. A region where the nucleate boiling occurs is defined as a nucleation site, which becomes larger in the upper part of the saddle as time advances. It is shown in Fig. 7 that the nucleate boiling triggered by the phase change phenomenon changes the volume fraction of the gas, and generates more vapors over time.

Figs. 8–10 shows the velocity vector field of the liquefied gas in a streamline of instantaneous velocity and streamtube, where a varying color represents the magnitude and the strength of vertical component of the velocity. Overall, the trends of the flow in the domains of the vapor and the liquid region show large discrepancy. In the liquid, thermal convection with a pair of vortex longitudinally-large in the horizontal plane is observed mostly due to the external heat transferred from the environment outside. As time proceeds, uprising motion of the vapor in the vertical direction becomes more complicated in the upper part of the saddle, which affects the flow patterns of convective heat transfer. In the domain of vapor state, the thermal convection, which is caused by the high-temperature liquids on the saddle, is focused around the center of the vapor–liquid contact surface, contains vapors moving upwards, and forms a pair of primary vortices of large size in vertical plane. In addition, liquids in thermal convection moves upwards to the upper part of the liquid–vapor interface along the interior surface of the tank. At the same time, there exists thermal convection with flows moving downward due to the primary vortex, which then creates the secondary vortex in vertical plane. As time passes, the thermal convection in the upper part of the vapor state domain reduces due to high temperature on the upper surface of the tank outside, however; convection in all other domains develops with increasing magnitude.

Next, changes in the mass of vapor due to the phase change is calculated and compared with the experimental data [33] as shown in Fig. 11. The present study calculates the time rate of reduction in mass to be 2.52 kg/hour, while the experiment predicts 2.28 kg/hour

In Fig. 12, comparison of the BOR values based on the BOG estimated by Eqs. (17) and (19) is carried out with the experiments by Lin et al [33] and those by the thermal analysis of FEM where the fluid domain is assumed to be rigid. First, the BOR_Q which is calculated by the present study in consideration of the thermal convection only and without the phase change is underestimated by −3.43% when compared to the experiment, whereas the FEA calculated by Lin et al. [33] does not consider the thermal convection and leads to the relative error of −3.9% in the BOR_Q. However, if the phase change model is included in the present study, the relative error in the BOR_Q values is as small as 0.14% and closer to the experiments. In order to accurately calculate BOR_Q, the value of Q_{leak} must be correct. This is because, as shown in Eq. (17), in the coefficient values included in BOR_Q, Q_{leak} is a variable and the remaining are defined as constant values. Eq. (18) can be used to estimate Q_{leak}. Table 7 shows the difference of Q_{leak} in reference to the experiment [33] in two numerical simulations. In the simulations where the phase change model was not used, the difference value was 5.3 W and 4.75 W for Lin et al.'s and present models, respectively. These discrepancies from the experiment value are reported to be caused by the neglecting of the convection details in the calculation [33]. However, when the phase change model is applied to the present simulation, a difference value as small as 0.47 W are calculated and the physics of flow convection flow is adequately modeled.

The improved accuracy is due to the fact that the calculation with the phase change model can precisely resolve the multiple physics of the liquefied gas, where the time rate of volume change becomes different corresponding to the phase changes in the cryogenic tank, and affects the characteristics of liquids near the interface. The numerical calculation captures the effects of the heat conduction from the interior of the tank to gas/fluids in multiple phases, which eventually changes the total heat flux. On the other hand, the value of BORv calculated based on the BOG shows the relative error of −0.83%, which is less than the value of BOR_Q by 0.9%.

Overall, it is obvious that the CFD-based simulation enables thorough understanding on the phase change process of the liquefied gas in the cryogenic tank due to the heat transfer penetrating the insulation from the external environment and resultant heat convection inside the tank. Detailed information on the multiple physics of the liquefied gas inside the tank is critical to the minimization of the heat loss of the entire system, development of an efficient insulation system, and the design of an energy-efficient cryogenic storage system.

3.2. Application case: Membrane-type LNG tank

3.2.1. Simulation model

Based on the validation of the phase change model used in the CFD simulation of the cryogenic liquefied LN_2 gas in the type-C storage tank, the estimation of the BOR values is carried out for the KC-1 LNG membrane-type tank which was developed by Korea Gas Corporation, KOGAS. The geometry of the tank and the information on the insulation system are shown in Fig. 13 and are referred to the study by Jeong et al.

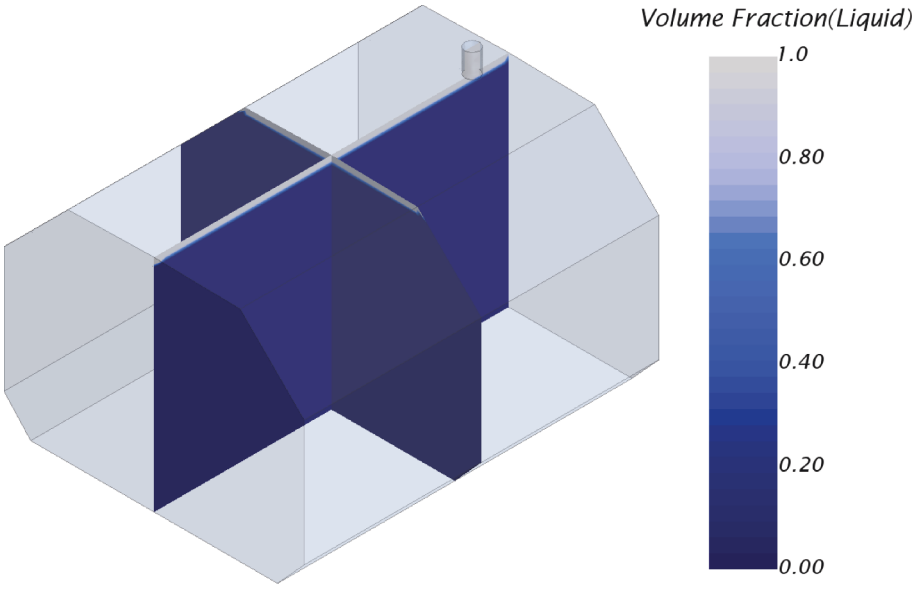

(a) Volume of fraction

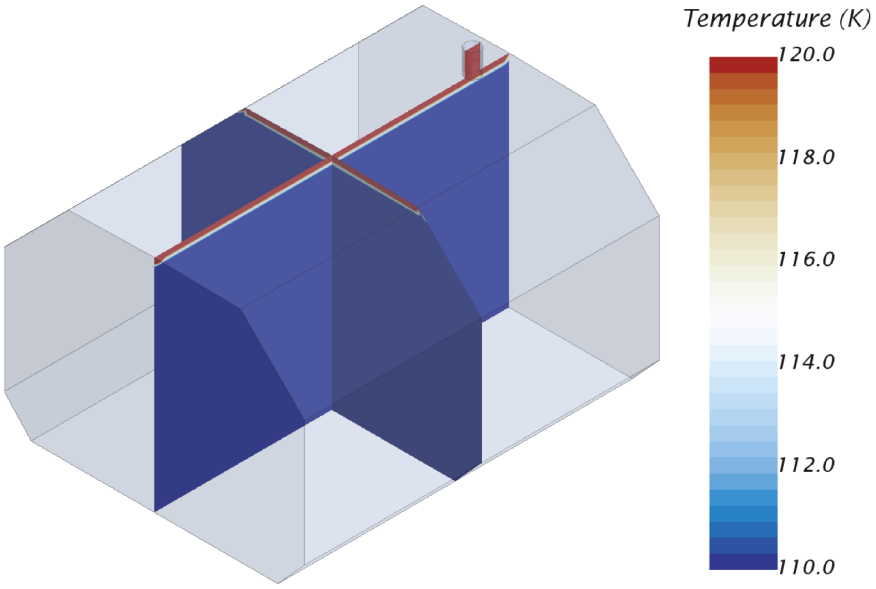

(b) Temperature

Fig. 16. Initial setup of volume fraction and temperature for KC-1 LNG tank.

[20]. However, the insulation system, shown in Fig. 13(b), consists of complicated substructures of different materials. Material properties for each of them are shown in Table 8, and assumed in the present study to be homogeneous and calculated as an equivalent parameter by the formulation as follows.

$$f_{eq} = \sum_{i=1}^{n} \frac{f_1 V_1 + f_2 V_2 + \cdots + f_n V_n}{V_t}, \tag{21}$$

where $f_1, f_2, \cdots, f_n$ represents the material property of the component of the insulation system, and $V_1, V_2, \cdots, V_n$ corresponds to the volume of an individual component, where $V_t = V_1 + V_2 + \cdots + V_n$.

Using this equivalent parameter in Eq. (21), it is possible to define the amount of heat transfer from the inner hull of the tank to the surface of the LNG by a single parameter to represent heat resistance.

3.2.2. Simulation condition

For the calculation to estimate the BOR values in consideration of the phase change in the LNG tank, the same conditions are used as in the FEM-based thermal analysis carried out by Jeong et al. [20]. Substructures of the hulls and compartment are neglected for the simplicity of the CFD simulation. The temperature distribution on the outer surface of the insulation shown in Fig. 14 is set by the values obtained in the study by Jeong et al. [20], and summarized in Table 9. The tank contains the LNG and the natural gas, and their material properties are shown in Tables 10 and 11 with the initial temperatures listed in Table 12.

A computational mesh used in the CFD simulation is shown in Fig. 15

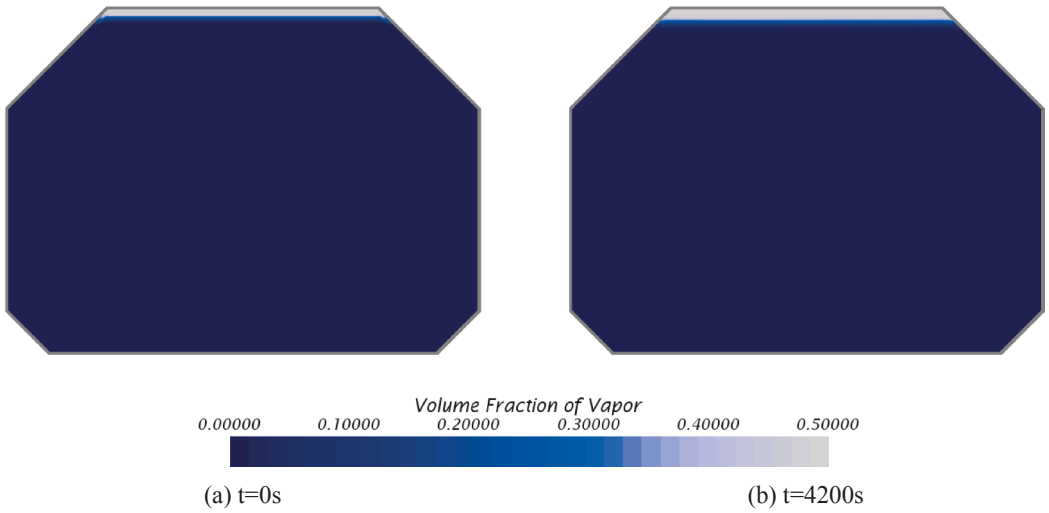

Fig. 17. Volume fraction of natural gas in KC-1 tank at different time.

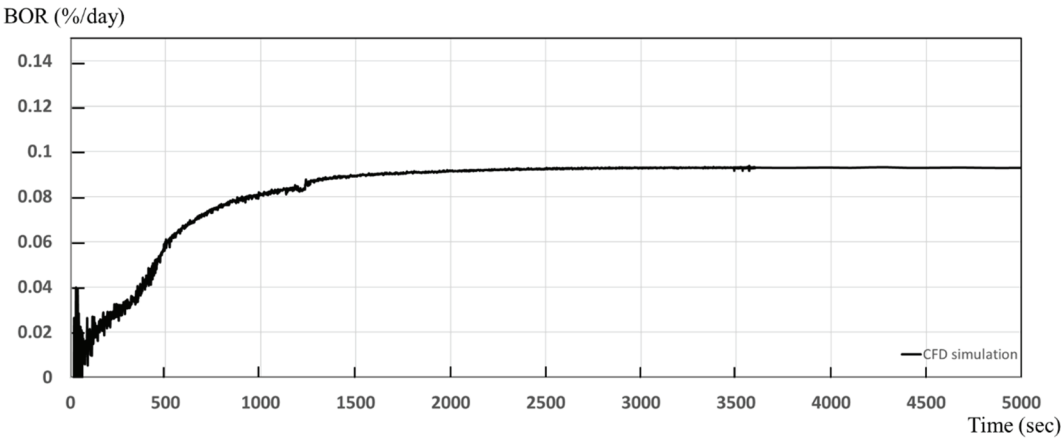

Fig. 18. BOR in KC-1 tank along with time.

with the total number of grid cells of 5.5 million. Meshes for the subdomains of fluids and solids are generated separately with the condition of Conjugate Heat Transfer applied on the interface of the subdomains.

Fig. 16 shows the initial state of the LNG tank of 98% loading, with its volume fraction and temperature shown in Fig. 16(a) and (b), respectively. The CPU time for the entire calculation was 6 days using 980 cores of Intel Xeon Platinum 8168 scalable processor with 2.70 GHz frequency with the Massively Parallel Interface (MPI) library.

3.2.3. *Simulation results*

To investigate the changes in the amount of BOG inside the membrane-type LNG tank when the phase change model is applied for the CFD simulation, the volume fractions of vapors at two different times of 0 and 4200 s are calculated and shown in Fig. 17(a) and (b), respectively. The amount of vapor at t = 4200 s seems to be increased when compared to the initial state. In Fig. 18, Boil-off rate in KC-1 LNG tank is shown. A gradual increase in BOR with fluctuations is obtained until 1500 s, but the constant BOR is observed afterwards.

To investigate the distribution of temperature in equilibrium after t = 1000 s when the amount of vapor is generated at a constant rate, the temperature on the insulation and the internal fluids is shown in Fig. 19 (a) and (b) in front and side views, respectively. For the temperature distribution on the insulation, external temperature outside the upper part of the insulation is higher than that of the lower part, and the distribution is determined by the temperature difference between the interior and the exterior of the insulation. Cofferdam are installed in the front and rear parts of the tank and the initial temperature is set 3.06 degree based on the study by Jeong et al. [20]. On the bottom of the side of the tank, the initial temperature is set 27.64°, which appears to cause the temperature discrepancies. For better understanding, the temperature distribution on the insulation for each part of the insulation is shown in Fig. 19(c).

A dynamic behavior of the liquefied gas from the thermal convection inside the LNG tank is shown in Fig. 21 in terms of the velocity field in LIC at t = 100, 300, 500, 700, 1000, and 1500 s. In Fig. 21(a), early in the CFD simulation, heat energy is transferred into the boundary layer by the thermal conduction from the both sides of the insulation. Based on the Buoyancy-Driven Two-Layer type model for the boundary layer flows, fluids experience the buoyancy force, form jet stream moving upwards, and cause convective heat transfer. During the convection, some portions of the liquids vaporize and the rest are cooled down forming the flows moving downwards near to the interface of liquid–vapor. In Fig. 20(b), ascending flows become more active in the convection on the sidewall of the tank, and the heat transfer becomes very strong from the upper corners of the tank, which h makes LNG boil, increases the convection speed, and disturb the fluids on the upper part.

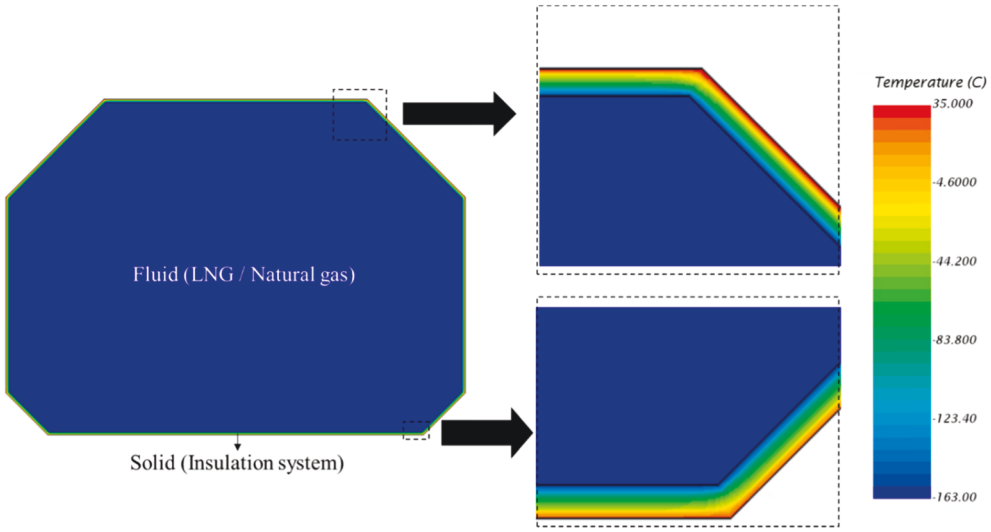

(a) Front view

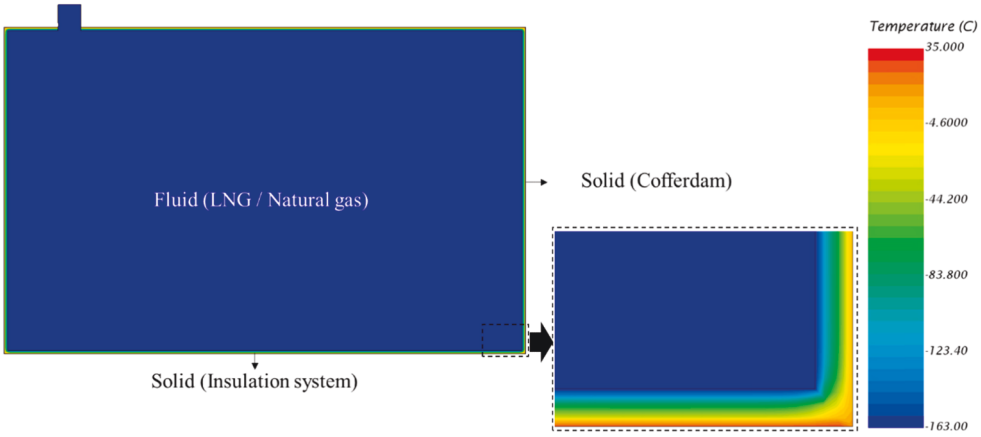

(b) Side view

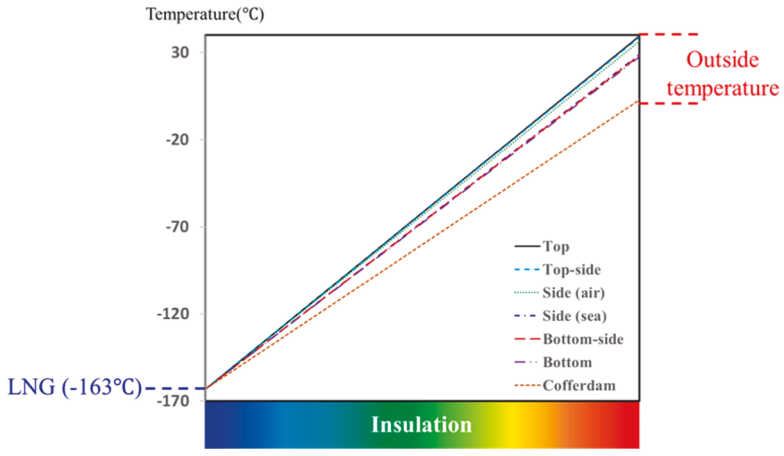

(c) Temperature distribution in insulation

Fig. 19. Temperature distribution of insulation and LNG at t = 1000 s.

However, in the center of the tank, the LNG is cooled down on the interface of the LNG and the natural gas (vapor–liquid interface) and generates descending flows. On the other hand, random boiling of the LNG is observed along the bottom of the tank due to the heat transferred to the insulation from the external environment. In Fig. 20(c)–(e), jet streams ascending due to the heat transferred from the sidewalls of the LNG tank are cooled down to disappear. However, the convection continues in the vapor–liquid interface, and some LNG are seen to be

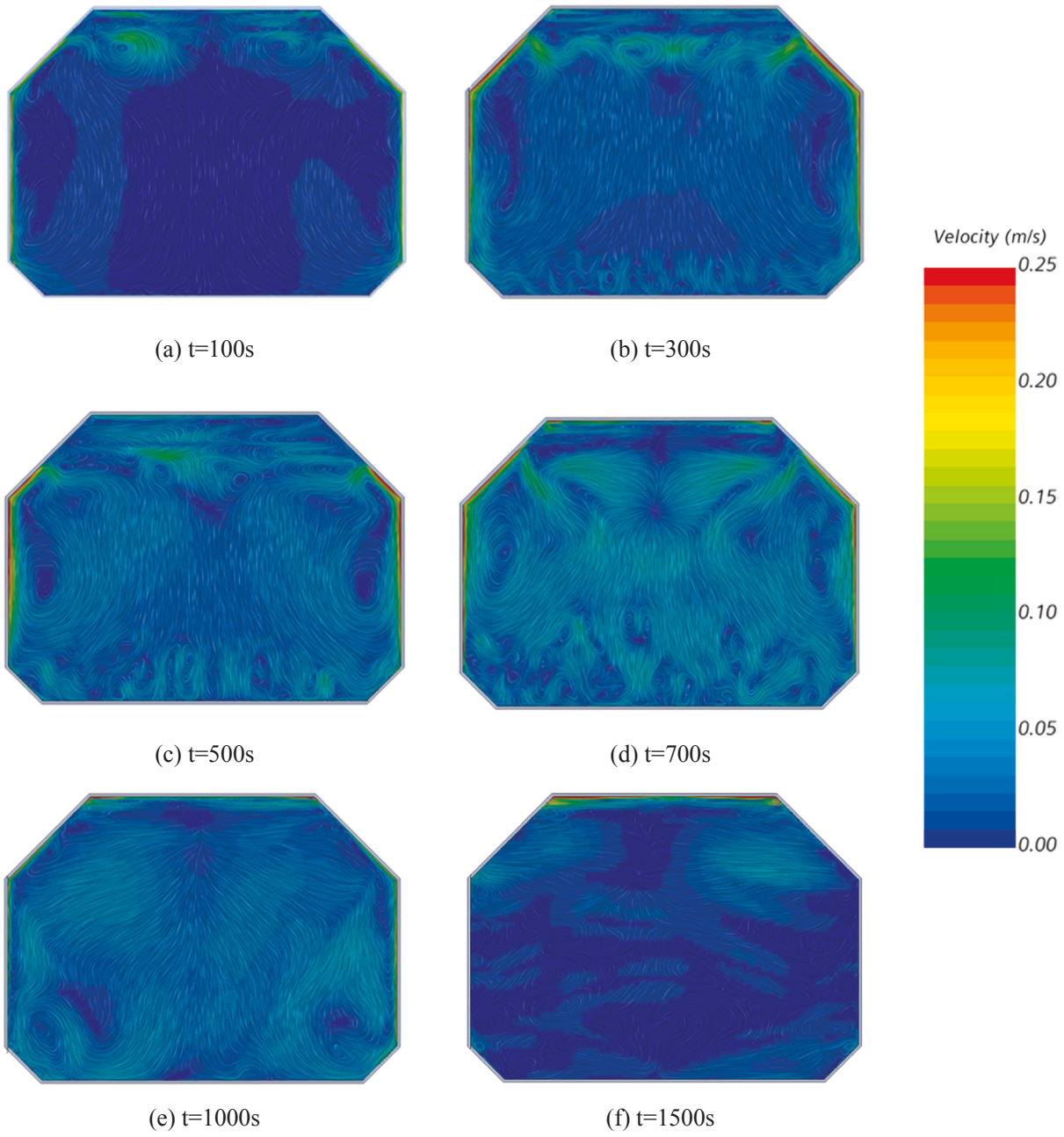

Fig. 20. Time-sequential heat convection flow in LNG tank (Front view).

vapored. This is observed in Fig. 21(f) where the fluids in the LNG areas are cooled sufficiently after 1500 s enough to make the convection disappear. However, in the vapor areas near the vapor–liquid interface and upper corners of the tank, the convection seems to continue due to the vaporization. Excessive heat transfers around the upper corner areas are thought to be due to the numerical assumption of a single value for all thermal conductivity parameters for the insulation. .

3.2.4. Comparison of BOR

In this section, the BOR values calculated by the present study is compared with the values of BOR_Q calculated by previous studies [34,45,20] using the total heat transfer, although the geometry of the membrane-type LNG tank is not exactly the same. Comparison results are summarized in Table 13 in terms of the author of the study, CFD software used, and the use of the phase change model. The present study also carried out a separate simulation to calculate the BOR_Q values using the total heat transfer for the comparison purpose, and the resultant BOR_Q is compared with that of the previous studies and summarized in Table 14. The resultant BOR_Q value from our study is 0.0972%/day, and is within the range of 0.0856%/day to 0.0986%/day suggested by other numerical simulations. When compared with the result of the study by Jeong et al. [20] which used the same conditions for the thermal analysis, the value of BOR_Q is slightly lower by 1.4%.

The amount of vapor generated for an hour is calculated by $m^3/hour$ and listed in Table 15. The corresponding BOR value is calculated to be 0.093%/day by Eq. (18). As shown in Fig. 21, although the simulation results of Yu et al. [45] employed the phase change model, but underpredicts the vaporization with the lower BOR values than those of the numerical simulation carried out by other researchers. It is shown that the predicted results of BOR values by the present study is within the

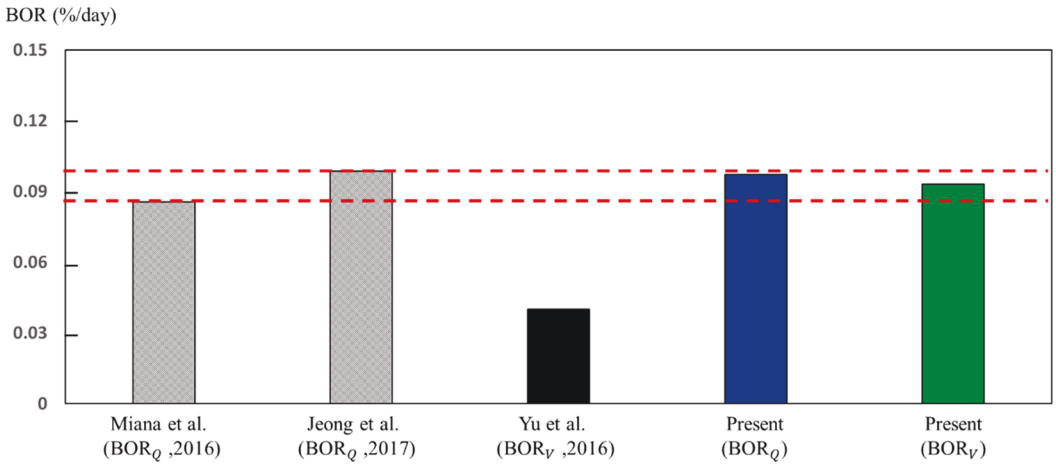

Fig. 21. Comparison of BOR with other data.

Table 13
Specification of LNG tank simulated by authors.

Authors	CFD code	Phase change model
Miana et al. [34]	Fluent	X
Yu et al. [45]	STAR-CCM+	O
Jeong et al. [20]	Fluent	X
Present	STAR-CCM+	O

Table 14
Specification of LNG tank simulated by authors.

Authors	BOR_Q (%/day)
Miana et al. [34]	0.0856
Jeong et al. [20]	0.0986
Present	0.0972

Table 15
Specification of LNG tank simulated by authors.

Authors	Loss of LNG volume (m^3/hour)	BOR_V (%/day)
Yu et al. [45]	220	0.04
Present	512	0.093

Table 16
Comparison with BOR_Q and BOR_V.

	BOR_Q (%/day)	BOR_V (%/day)	Difference (%)
Present	0.0972	0.093	4.3

range of published predictions.

The resultant values of BOR_Q and BOR_V calculated by the present method are summarized in Table 16 with 4.3% difference where the BOR_V is predicted slightly less than the BOR_Q. However, results of improved accuracy are calculated, confirming that the phase change model is critical in the calculation to the precise estimation of the BOR values.

4. Concluding remarks

The multi-physics CFD simulation was carried out for the precise estimation of the BOG and BOR values necessary to the design of CCS for the cryogenic liquid. It considers the phase change of liquefied gas as well as the heat transfer in the insulation system, is more advantageous that the traditional method which considers the total heat transfer only and does not take into account the actual physics of phase change inside the cryogenic tank. Conclusions are as follows from the comparison of the BOR values predicted by the method using the total heat transfer only, with the BOR values calculated by the present CFD method based on the BOG amount estimated from the phase change of the liquid.

(1) The vaporization of the cryogenic liquid on the interface with the vapor is accurately calculated by the phase change model implemented in the VOF model. First, to investigate the applicability of the phase change model, the results of the BOR and BOG values were compared with those of the existing study by Lin et al. [33], and show that the present method can provide reliable predictions by detailed analysis of the cryogenic liquid inside the tank which undergoes the phase change.

(2) The natural convection and the phase change phenomena inside the type C tank are well resolved by the present method, which cannot be explained in detail by the experiments. It is understood from the present calculations that the phase change occurs by the external heat transfer on the saddle support due to its high thermal conductivity as well as on the interface of liquid and vapor. The present study calculates the BOR values based on the total heat transfer and on the amount of vapor, i.e., BOG. When the BOR value is predicted by the method using the phase change model and compared with the experiments, the relative error becomes less than 1%, which demonstrates the advantage of the phase change model.

(3) To extend the application of the phase change model, the value of BOR is calculated based on the amount of vaporization of the LNG due to the external heat transfer to the insulation of the LNG membrane tank which was developed by KOGAS. The convection is observed to be continuous on the interface of the liquid and vapor, and the movement of flow caused by convection in the area of the LNG gradually disappear as LNG becomes cooled down over time. On the other hand, in vapor region, the convection continues near the upper corners of the tank and on the vapor–liquid interface, which may be attributed to the numerical artifacts of the single thermal conductivity of the insulation for the sake of simplicity in the computation making the insulation susceptible to the external heat transfer. The BOR prediction in consideration of the true physics is compared with that of the other simulations based on the total heat transfer only [34,20], showing good agreements with the relative error less than 1.4% with respect to the results of Jeong et al. [20] which used the same test case. It is concluded that the calculation results of the BOR carried out by the present method based on the amount of vapor are able to provide great improvement in accuracy from the previous studies by other researchers [45], and demonstrates

great potential in the BOR prediction method based on the phase change model. In other words, the heat convection of the fluid considering the phase change of liquid as well as the heat conduction of the solid were simultaneously implemented, and this could take a step closer to the reproduction of more practical physical phenomena.

For future works, a variety of applications at various conditions must be calculated using the proposed phase change model in order to verify the validity of the method. The present calculation is validated with existing experiments and validation with practical physics where complex interacting phenomena are taking place. After then, many industrial application problems, such as loading/unloading problems of cryogenic liquids accompanying the time change, heat loss problems of local support structures, dynamics problems with sloshing during operation will be solved by the CFD simulation. The high-fidelity CFD-based calculation method will be greatly beneficial to the analysis, design, and the development of the Korea LNG tank system. In addition, the method can be further applied to engineering areas which uses liquid hydrogen gas including ships, cars and spacecraft.

Declaration of Competing Interest

The authors declare that they have no known competing financial interests or personal relationships that could have appeared to influence the work reported in this paper.

Acknowledgement

This research was a part of the project titled 'Development of Safety and Control Standards for Hydrogen Ships: Cargo Handling and Fuel Gas Supply Systems', funded by the Ministry of Oceans and Fisheries, Korea.

References

[2] M. Ahammad, Y. Liu, T. Olewski, L.N. Véchot, M.S. Mannan, Application of computational fluid dynamics in simulating film boiling of cryogens, Ind. Eng. Chem. Res. 55 (2016) 7548–7557, https://doi.org/10.1021/acs.iecr.6b01013.
[4] R. Banerjee, A numerical study of combined heat and mass transfer in an inclined channel using the VOF multiphase model, Numer. Heat Transfer A Appl. 52 (2007) 163–183, https://doi.org/10.1080/10407780601149862.
[5] R. Banerjee, Turbulent conjugate heat and mass transfer from the surface of a binary mixture of ethanol/iso-octane in a countercurrent stratified two-phase flow system, Int. J. Heat Mass Transf. 51 (2008) 5958–5974, https://doi.org/10.1016/j.ijheatmasstransfer.2008.04.057.
[6] M. Belmedani, A. Belgacem, R. Rebiai, Analysis of Natural convection in liquid nitrogen under storage conditions, J. Appl. Sci. 8 (2008) 2544–2552, https://doi.org/10.3923/jas.2008.2544.2552.
[7] D. Boukeffa, M. Boumaza, M.X. Francois, S. Pellerin, Experimental and numerical analysis of heat losses in a liquid nitrogen cryostat, Appl. Therm. Eng. 21 (2001) 967–975, https://doi.org/10.1016/S1359-4311(00)00098-3.
[8] S.J. Cha, J.H. Bae, D.H. Lee, T.W. Kim, S.K. Kim, J.M. Lee, Experimental analysis of boil-off gas occurrence in independent liquefied gas storage tank, J. Ocean Eng. Technol. 32 (2018) 380–385, https://doi.org/10.26748/KSOE.2018.6.32.5.380.
[9] T.W. Chen, A new approach of computational fluid dynamics studying power transient critical heat flux. https://doi.org/10.1016/j.energy.2019.02.098.2019 (accessed 14 July 2020).
[11] J.L. Ferrín, L.J. Pérez-Pérez, Numerical simulation of natural convection and boil-off in a small size pressurized LNG storage tank, Comput. Chem. Eng. (2020) 106840, https://doi.org/10.1016/j.compchemeng.2020.106840.
[12] J. Fu, B. Sunden, X. Chen, Y. Huang, Influence of phase change on self-pressurization in cryogenic tanks under microgravity, Appl. Therm. Eng. 87 (2015) 225–233, https://doi.org/10.1016/j.applthermaleng.2015.05.020.
[13] GIIGNL Technical Study Group, Rollover in LNG Storage Tanks, Technical report, 2015. https://giignl.org/sites/default/files/PUBLIC_AREA/Publications/rollover_in_lng_storage_tanks_public_document_low-res.pdf (accessed 14 July 2020).
[14] K.C. Han, S.W. Hwang, J.R. Cho, J.S. Kim, J.W. Yoon, O. Lim, S.B. Lee, A study on the boil-off rate prediction of LNG cargo containment filled with insulation powders, J. Comput. Struct. Eng. Inst. Korea 24 (2011) 193–200.
[16] A. Hassanvand, S.H. Hashemabadi, M. Bayat, Evaluation of gasoline evaporation during the tank splash loading by CFD techniques, Int. Commun. Heat Mass 37 (2010) 907–913, https://doi.org/10.1016/j.icheatmasstransfer.2010.05.011.
[17] C.M. Hwang, Y.S. Lim, Optimal process design of onboard BOG Re-liquefaction System for LNG Carrier, J. Ocean Eng. Technol. 32 (2018) 372–379.
[18] T. Höhne, E. Krepper, G. Montoya, D. Lucas, CFD-simulation of boiling in a heated pipe including flow pattern transitions using the GENTOP concept, Nucl. Eng. Des. 322 (2017) 165–176, https://doi.org/10.1016/j.nucengdes.2017.06.047.
[19] F. Huerta, V. Vesovic, A realistic vapour phase heat transfer model for the weathering of LNG stored in large tanks, Energy 174 (2019) 280–291, https://doi.org/10.1016/j.energy.2019.02.174.
[20] H.W. Jeong, T.H. Kim, S.S. Kim, W.J. Shin, Thermal Analysis of Insulation system for KC-1 Membrane LNG Tank, J. Ocean Eng. Technol. 31 (2017) 91–102, https://doi.org/10.5574/KSOE.2017.31.2.091.
[22] K.K. Jin, I.S. Yoon, Y.C. Yang, An effect of surface dashpot for KC-1 basic insulation system under sloshing loads, Trans. Korean Soc. Mech. Eng. C. Ind. Technol. Innov. (2015), https://doi.org/10.3795/KSME-C.2015.3.3.193.
[23] T. Kanazawa, K. Kudo, A. Kuroda, N. Tsui, Experimental study on heat and fluid flow in LNG tank heated from the bottom and the sidewalls, Heat Transfer Asian Res. 33 (2004) 417–430, https://doi.org/10.1002/htj.20031.
[24] O. Khemis, M. Boumaza, M.A. Ali, M.X. Francois, Experimental analysis of heat transfers in a cryogenic tank without lateral insulation, Appl. Therm. Eng. 23 (2003) 2107–2117, https://doi.org/10.1016/S1359-4311(03)00164-9.
[25] O. Khemis, R. Bessaïh, M.A. Ali, M.X. Francois, Measurement of heat transfers in cryogenic tank with several configurations, Appl. Therm. Eng. 24 (2004) 2233–2241, https://doi.org/10.1016/j.applthermaleng.2004.02.002.
[26] D. Kim, C. Hwang, T. Gundersen, Y. Lim, Process design and economic optimization of boil-off-gas re-liquefaction systems for LNG carriers, Energy 173 (2019) 1119–1129, https://doi.org/10.1016/j.energy.2019.02.098.
[27] E. Krepper, B. Končar, Y. Egorov, CFD modelling of subcooled boiling—concept, validation and application to fuel assembly design, Nucl. Eng. Des. 237 (2007) 716–731, https://doi.org/10.1016/j.nucengdes.2006.10.023.
[28] E. Krepper, R. Rzehak, CFD for subcooled flow boiling: Simulation of DEBORA experiments, Nucl. Eng. Des. 241 (2011) 3851–3866, https://doi.org/10.1016/j.nucengdes.2011.07.003.
[29] R.N. Krikkis, A thermodynamic and heat transfer model for LNG ageing during ship transportation. Towards an efficient boil-off gas management, Cryogenics (2018), https://doi.org/10.1016/j.cryogenics.2018.04.007.
[30] M. Langari, Z. Yang, J.F. Dunne, S. Jafari, J.P. Pirault, C.A. Long, J. Thalackottore Jose, Conjugate heat transfer predictions for subcooled boiling flow in a horizontal channel using a volume-of-fluid framework, J. Heat Transfer (2018), https://doi.org/10.1115/1.4040358.
[31] J.H. Lee, H.K. Choi, S. Choi, C. Oh, M.H. Kim, K.K. Kim, Thermal analysis for the GT-96 membrane type LNGC during the cool-down period, Proc. Korean Soc. Mech. Eng. (2004) 1346–1351.
[32] J.H. Lee, Y.J. Kim, S. Hwang, Computational study of LNG evaporation and heat diffusion through a LNG cargo tank membrane, Ocean Eng. 106 (2015) 77–86, https://doi.org/10.1016/j.oceaneng.2015.06.045.
[33] Y. Lin, C. Ye, Y.Y. Yu, S.W. Bi, An approach to estimating the boil-off rate of LNG in type C independent tank for floating storage and regasification unit under different filling ratio, Appl. Therm. Eng. 135 (2018) 463–471, https://doi.org/10.1016/j.applthermaleng.2018.02.066.
[34] M. Miana, R. Legorburo, D. Díez, Y.H. Hwang, Calculation of boil-off rate of liquefied natural gas in mark III tanks of ship carriers by numerical analysis, Appl. Therm. Eng. 93 (2016) 279–296, https://doi.org/10.1016/j.applthermaleng.2015.09.112.
[35] S. Nukiyama, An experiment on the atomization of liquid by means of an air stream (1), J. Soc. Mech. Eng., Jpn. 4 (1938) 128–135.
[36] Y. Qu, I. Noba, X. Xu, R. Privat, J.N. Jaubert, A thermal and thermodynamic code for the computation of boil-off gas-industrial applications of LNG carrier, Cryogenics 99 (2019) 105–113, https://doi.org/10.1016/j.cryogenics.2018.09.002.
[37] W.E. Ranz, W.R. Marshall, Evaporation from drops, Chem. Eng. Prog. 48 (1952) 141–146.
[38] W.M. Rohsenow, A method of correlating heat transfer data for surface boiling liquids, Trans. ASME 74 (1952) 969.
[39] A. Saleem, S. Farooq, I.A. Karimi, R. Banerjee, A CFD simulation study of boiling mechanism and BOG generation in a full-scale LNG storage tank, Comput. Chem. Eng. 115 (2018) 112–120, https://doi.org/10.1016/j.compchemeng.2018.04.003.
[40] T.H. Shih, W.W. Liou, A. Shabbir, Z. Yang, J. Zhu, A new k-epsilon eddy viscosity model for high Reynolds number turbulent flows, Comput. Fluids 24 (1995) 227–238.
[41] Siemens, STAR-CCM+ User Guide, Version 13.06.
[42] T.A.M. Versteegh, F.T.M. Nieuwstadt, A direct numerical simulation of natural convection between two infinite vertical differentially heated walls scaling laws and wall functions, Int. J. Heat Mass Transf. 42 (1999) 3673–3693, https://doi.org/10.1016/S0017-9310(99)00037-X.
[43] G. Wei, J. Zhang, Numerical study of the filling process of a liquid hydrogen storage tank under different sloshing conditions, Processes 8 (9) (2020) 1020, https://doi.org/10.3390/pr8091020.
[44] S. Wu, Y. Ju, J. Lin, Y. Fu, Numerical simulation and experiment verification of the static boil-off rate and temperature field for a new independent type B liquefied natural gas ship mock up tank, Appl. Therm. Eng. (2020) 115265, https://doi.org/10.1016/j.applthermaleng.2020.115265.
[45] K. Yu, Z. Ge, R. Korpus, CFD predictions of FLNG BOG including the influence of filling, offloading, and vessel motion, in: Offshore Technology Conference, 2016, https://doi.org/10.4043/27228-MS.
[46] M.S. Zakaria, K. Osman, M.N.A. Saadun, M.Z.A. Manaf, M. Hanafi, M. Hafidzal, Computational simulation of boil-off gas formation inside liquefied natural gas tank using evaporation model in ANSYS fluent, Appl. Mech. Mater (2013), https://doi.org/10.4028/www.scientific.net/AMM.393.839.

[47] R. Zhou, W.L. Zhu, Z. Hu, S. Wang, H. Xie, X. Zhang, Simulations on effects of rated ullage pressure on the evaporation rate of liquid hydrogen tank, Int. J. Heat Mass Transf. 134 (2019) 842–851, https://doi.org/10.1016/j.ijheatmasstransfer.2019.01.091.

[48] S. Zhu, Y. Li, X. Zhi, C. Gu, Y. Tang, L. Qiu, Numerical analysis of nitrogen condensation heat transfer enhancement with liquid film fluctuation at cryogenic temperature, Int. J. Heat Mass Transf. 149 (2020) 119151, https://doi.org/10.1016/j.ijheatmasstransfer.2019.119151.

[49] Z. Zuo, W. Jiang, X. Qin, Y. Huang, Numerical investigation on full thermodynamic venting process of liquid hydrogen in an on-orbit storage tank, Int. J. Hydrog. Energy (2020).